AGU PUBLICATIONS

JGR

Journal of Geophysical Research: Space Physics

RESEARCH ARTICLE

10.1002/2013JA019477

Key Points:
- Flapping modes may be separated by the analysis of plasma velocity
- The velocity vector rotates different for the kink and sausage modes
- The mode's separation strongly depends on noise and multiple sources existence

Correspondence to:
D. I. Kubyshkina,
kubyshkina.darya@gmail.com

Citation:
Kubyshkina, D. I., D. A. Sormakov, V. A. Sergeev, V. S. Semenov, N. V. Erkaev, I. V. Kubyshkin, N. Y. Ganushkina, and S. V. Dubyagin (2014), How to distinguish between kink and sausage modes in flapping oscillations?, *J. Geophys. Res. Space Physics*, *119*, 3002–3015, doi:10.1002/2013JA019477.

Received 24 SEP 2013
Accepted 7 APR 2014
Accepted article online 9 APR 2014
Published online 29 APR 2014

How to distinguish between kink and sausage modes in flapping oscillations?

D. I. Kubyshkina[1], D. A. Sormakov[2], V. A. Sergeev[1], V. S. Semenov[1], N. V. Erkaev[3,4], I. V. Kubyshkin[1], N. Yu. Ganushkina[5,6], and S. V. Dubyagin[5]

[1]Faculty of Physics, Earth Physics Department, Saint Petersburg State University, Saint Petersburg, Russia, [2]Arctic and Antarctic Research Institute, Saint Petersburg, Russia, [3]Institute of Computational Modelling SB RAS, Krasnoyarsk, Russia, [4]Department of Applied Mechanics, Polytechnic Institute, Siberian Federal University, Krasnoyarsk, Russia, [5]Finnish Meteorological Institute, Helsinki, Finland, [6]Department of Atmospheric, Oceanic and Space Sciences, University of Michigan, Ann Arbor, Michigan, USA

Abstract Flapping waves are most noticeable large-scale perturbations of the magnetotail current sheet, whose nature is still under discussion. They represent rather slow (an order of magnitude less than typical Alfven speed) waves propagating from the center of the sheet to its flanks with a typical speed of 20–60 km/s, amplitude of 1–2 R_e and quasiperiod of 2–10 min. The double-gradient MHD model, which was elaborated in Erkaev et al. (2007) predicts two (kink and sausage) modes of the flapping waves with differences in their geometry and propagation velocity, but the mode structure is hard to resolve observationally. We investigate the possibility of mode identification by observing the rotation of magnetic field and plasma velocity vectors from a single spacecraft. We test theoretical results by analyzing the flapping oscillations observed by Time History of Events and Macroscale Interactions during Substorms spacecraft and confirm that character of observed rotation is consistent with kink mode determination made by using multispacecraft methods. Also, we checked how the existence of some obstructive conditions, such as noise, combined modes, and multiple sources of the flapping oscillations, can affect on the possibility of the modes separation with suggested method.

1. Introduction

Flapping oscillations, the fast vertical motions of the Earth's magnetotail plasma sheet, were observed since long time ago [e.g., *Ness*, 1965], but only Cluster mission was able to fully reveal the main signatures of this phenomenon [e.g., *Zhang et al.*, 2002; *Sergeev et al.*, 2003, 2004, 2006a; *Runov et al.*, 2005, 2006; *Petrukovich et al.*, 2006; *Shen et al.*, 2003]. According to these observations, flapping oscillations represent waves, observed more frequently in the central part of the tail than near the flanks, which propagate from the midnight meridian to the flanks with the speed of 20–60 km/s (an order of magnitude less than a typical Alfvén velocity), amplitude of 1–2 R_e and quasiperiod of 2–10 min. These flapping motions are probably caused by some transient process localized in the magnetotail center. They were also founded in the magnetospheres of Jupiter and Saturn [*Volwerk et al.*, 2013].

There exist several theoretical explanations of the flapping oscillations in the Earth's magnetotail. The Drift-Kink Instability (DKI) [*Daughton*, 1998, 1999; *Zelenyi et al.*, 2009] considers the relative drift of ions and electrons which is proposed to be the main driver of the flapping waves. Similar kink mode can be driven by the relative streaming between two populations of ion species (the cold lobe ions and the current-carrying hot plasma sheet ions) [*Daughton*, 1999], which provide an effective shear into the ion velocity profile. This instability is defined as ion-ion kink mode [*Karimabadi et al.*, 2003; *Sitnov et al.*, 2004] and grows faster than DKI. A similar approach is described in *Ricci et al.* [2004]: background ions create velocity shear, which in turn introduces Kelvin-Helmholtz instability and result in current sheet flapping motions. All this models belong to the drift modes, where oscillations propagate along the electric current. However, it should be noted, that the real flapping wave propagates both along and opposite the current.

In the magnetohydrodynamic (MHD) approach two models were elaborated. First, the ballooning-type mode in curvilinear magnetic field in the magnetotail current sheet was proposed by *Golovchanskaya and Maltsev* [2005]; for more details, see, e.g., *Mazur et al.* [2012]. They considered the wavelengths of the ballooning perturbations much less than curvature radius of magnetic field line in magnetotail. However, experimental data indicate that the wavelength of flapping oscillations is bigger than this curvature radius. (Thus, the frequency obtained in frame of ballooning model is different to the experimental one.)

The double-gradient (DG) model, which was elaborated by *Erkaev et al.* [2007, 2008, 2009a, 2009b, 2010]; *Artemyev and Zimovets* [2012], takes into account this fact. It was shown that frequency and wavelength of oscillations depend on the double gradient of magnetic field (gradient of B_x component on z and B_z component on x in GSM coordinate system). Relations between ballooning mode and DG mode was contemplated in detail in *Korovinskiy et al.* [2013]. Summarize, the double-gradient mode is a particular branch of a ballooning mode, when wavelength is bigger than curvature radius. Also, DG model was compared to the experimental data, and it was found that it is in a better accordance with experimental data than other models [see *Forsyth et al.*, 2009].

Two principal modes of the flapping motion exist in the double-gradient model. The kink mode is described by the even function for the z component of the displacement vector ξ_z with respect to Z, and the sausage mode is described by the odd function. If the satellite is located near the neutral plane then we can distinguish between these modes: B_x component changes its sign (then satellite crosses the neutral plane) for the kink mode, while for the sausage mode B_x preserve its sign and still close to zero value.

Most of the observed events were identified as the kink mode events [*Sergeev et al.*, 2006b] based on B_x sign change signature. At the same time the sausage mode can also exist. For instance, *Panov et al.* [2012] presented the event in which one of the Time History of Events and Macroscale Interactions during Substorms (THEMIS) probes was located in the central plasma sheet and observed B_x~0, when two other probes located at the current sheet periphery observed B_x oscillations with amplitudes exceeding 20 nT.

Previous attempts of mode determination strongly depended on the chance to have two probes in the current sheet both below and above of its center or to have the probe located right at the center of the current sheet. However, this is problematic in case of having the single spacecraft, or in the case of mixed modes.

In this paper we investigate the possibilities to distinguish between the modes (including the case of mixed modes) based on single point observations.

We review the double-gradient model of the flapping oscillations and propose the possible mechanism for the modes determination in section 2. Next, in section 3 we present the analysis of THEMIS probes observations for events on 5 March 2008 and 20 December 2007. Experimental data are compared with the theoretical predictions. In sections 4 and 5 we investigate the influence of the mixed modes and the noise, respectively. In the section 6 we present the modeling of the inverse gradient. The fast growth of small fluctuations corresponds to this case, and we propose the possible mechanism of the flapping waves appearance by means of short-duration intervals of inverse gradient.

2. Double-Gradient Model of the Flapping Oscillations

Flapping oscillations are a particular mode of the MHD waves in the magnetotail propagating across the magnetic field lines, which are much slower than the magnetosonic modes. As it was shown in [*Erkaev et al.*, 2009a] the incompressible approximation is appropriate in this case, and we can use the simplest system of incompressible ideal magnetohydrodynamic (MHD) equations

$$\rho\left(\frac{\partial \mathbf{v}}{\partial t} + (\mathbf{v}\cdot\nabla)\mathbf{v}\right) = -\nabla\Pi + \frac{1}{4\pi}(\mathbf{B}\cdot\nabla)\mathbf{B}; \tag{1}$$

$$\frac{\partial \mathbf{B}}{\partial t} + (\mathbf{v}\cdot\nabla)\mathbf{B} = (\mathbf{B}\cdot\nabla)\mathbf{v}; \tag{2}$$

$$\nabla\cdot\mathbf{v} = 0; \tag{3}$$

$$\nabla\cdot\mathbf{B} = 0. \tag{4}$$

Here $\mathbf{v}, \mathbf{B}, \rho, and\, \Pi = p + \frac{B^2}{8\pi}$ are the velocity, magnetic field, density, and total (plasma + magnetic) pressure, respectively. We concentrate our analysis on very slow wave modes existing only in the presence of magnetic field gradients. So we introduce the weak gradient $\frac{\partial B_z}{\partial x}$ and suppose that gradient $\frac{\partial B_x}{\partial z}$ exists but constant. All another derivations $\frac{\partial}{\partial x}$ are supposed to be zero, because magnetotail is the region with magnetic field much elongated in X direction. The configuration of the background magnetic field as well as the coordinate system is shown in Figure 1.

Following the standard procedure, we linearized the set of MHD equations (2)–(4). Since we are looking for the waves propagating in the Y direction, the perturbations are assumed to have the form

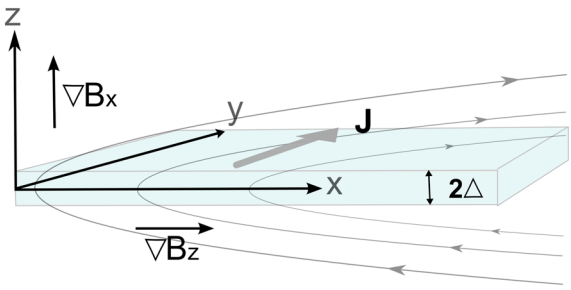

Figure 1. Schematic showing geometrical situation of the current sheet.

$\delta A(z)\exp(-i(\omega t - ky))$ where $\delta A(z)$ is the amplitude of a perturbation. Using the relation $v_z = -i\omega\xi_z$ we obtain one differential equation with the plasma displacement ξ_z as the variable

$$\frac{\partial^2\xi_z}{\partial z^2} + k^2\left(\frac{U^2(z)}{\omega^2} - 1\right)\xi_z = 0, \tag{5}$$

where k is the wave number in the Y direction, and $U^2(z)$ is equal to

$$U^2(z) = \frac{1}{4\pi\rho}\frac{\partial B_z}{\partial x}\frac{\partial B_x(z)}{\partial z}. \tag{6}$$

Here the gradient $\frac{\partial B_z}{\partial x}$ is supposed to be constant and $\frac{\partial B_x(z)}{\partial z}$ defines the structure of the current sheet. The function $\xi_z(z)$ has to vanish at large distances from the current sheet.

Solving the spectral equation (5) we can obtain eigenfrequency ω as a function of wave number k. In general case we have to solve the flapping boundary value problem numerically, but there exist several cases when it is still possible to obtain an analytical solution. One of them is the simplest configuration value problem of the current sheet with constant current density in the finite layer with thickness 2Δ [*Erkaev et al.*, 2007]. In spite of the fact, that this is a simplification of the real current sheet, the frequency, phase, and group velocities turn out to be close to those obtained from more realistic models. In this case, the equation (5) has a simple solution $\xi_z = D_1\cos(\lambda z) + D_2\sin(\lambda z)$ (where $\lambda = k^2(\frac{U^2}{\omega^2} - 1)$, $U = \text{const}$) for $|z| < \Delta$ and $\xi_z = Ce^{-k|z|}$ for $|z| > \Delta$. Choice of sinus or cosines in this solution is specified by the mode of flapping oscillations (even cosines corresponds to the kink mode, and odd sinus corresponds to the sausage mode). Since ξ_z and $\frac{\partial\xi_z}{\partial z}$ are continuous across the structure we can find the following transcendental equations for the kink and sausage modes, respectively:

$$\tan(\lambda) = \frac{k}{\lambda}, \quad \tan(\lambda) = -\frac{\lambda}{k}. \tag{7}$$

These equations have the discrete sequence of roots, the main root is the minimal λ which corresponds to the maximal frequency. Solving equations (7) numerically, we can obtain the dispersion relations, which are shown in Figure 2. It is convenient to approximate the dispersion relations with the following simple expressions for kink and sausage modes, respectively:

$$\omega_k(k) = 2\omega_f\frac{k\Delta + 0.15\sqrt{k\Delta}}{1 + 2k\Delta}; \tag{8}$$

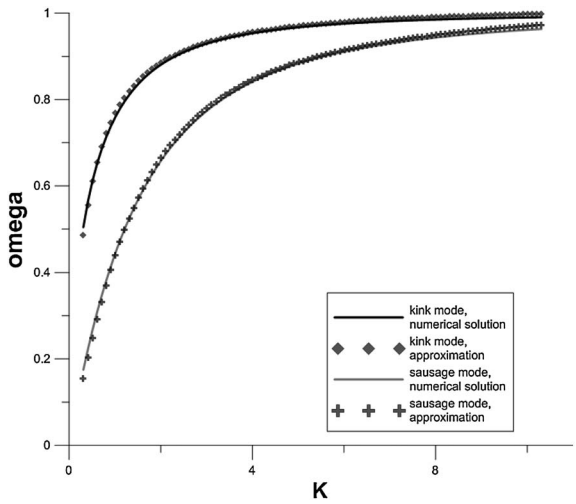

Figure 2. Dispersion curves for the kink and sausage wave modes and their approximations.

$$\omega_s(k) = \omega_f\frac{k\Delta(1 + k\Delta)}{2.14 + 1.7k\Delta + (k\Delta)^2}. \tag{9}$$

Here ω_f is the, so called, double-gradient frequency at z=0

$$\omega_f = \sqrt{\frac{1}{4\pi\rho}\left(\frac{\partial B_z}{\partial x}\frac{\partial B_x}{\partial z}\right)_{z=0}}. \tag{10}$$

Harris current sheet is another example providing the analytical solution [*Erkaev et al.*, 2009a, 2009b]. For this case the dispersion relations are

$$\omega_k(k) = \omega_f\sqrt{\frac{k\Delta}{k\Delta + 1}}; \tag{11}$$

$$\omega_s(k) = \omega_f\frac{k\Delta}{\sqrt{(k\Delta)^2 + 3k\Delta + 2}}. \tag{12}$$

As can be seen from Figure 2 both dispersion curves, kink, and sausage, asymptotically tend to the same limit which is double-gradient frequency (10). To illustrate the role of this frequency we consider the z component of the linearized equation of motion (2) and x component of the frozen-in equation (3)

$$\rho\frac{\partial v_z}{\partial t} = -\frac{\partial \delta\Pi}{\partial z} + \frac{1}{4\pi}\delta B_x\frac{\partial B_z}{\partial x}; \tag{13}$$

$$\frac{\partial \delta B_x}{\partial t} + v_z\frac{\partial B_x}{\partial z} = B_z\frac{\partial \delta v_x}{\partial z}. \tag{14}$$

The term $-\partial\delta\Pi/\partial z$ is responsible for the flux tube interaction and dispersion. In the limit $k \to \infty$ (thin flux tube approximation) this term becomes small. It was shown in *Erkaev et al.* [2009a, 2009b] that $v_x \sim B_z$ and right-hand side of the equation (14) is the term of the second order in B_z, and therefore, it can be neglected. Then the equations (13) and (14) lead to the equation for v_z

$$\frac{\partial^2 v_z}{\partial t^2} = -\frac{1}{4\pi\rho}\frac{\partial B_z}{\partial x}\frac{\partial B_x}{\partial z}\cdot v_z. \tag{15}$$

We can see that if $\frac{\partial B_x}{\partial z}\cdot\frac{\partial B_z}{\partial x} > 0$ the thin flux tube would oscillate up and down with the double-gradient frequency ω_f. In another case of inverse gradient $\frac{\partial B_x}{\partial z}\cdot\frac{\partial B_z}{\partial x} < 0$ there is an instability. This double-gradient instability has been investigated numerically in [*Korovinskyi et al.*, 2013] for the compressible set of MHD equations and it was shown that the dispersion curve obtained from simulations agrees with the theoretical dispersion curve within 10%.

Now we consider again the general case. To return from Fourier space to the real space we perform the inverse Fourier transformation with obtained dispersion relations. The Z component of the displacement vector is written as

$$\xi_z(t,y,z) = \frac{R_e}{2\pi}\int_{-\infty}^{\infty}\xi_z^0(k)\cos(\lambda(k)z)e^{i(\omega(k)t-ky)}\mathrm{d}k, \tag{16}$$

where $\lambda(k) = k\sqrt{\frac{U^2}{\omega^2}-1}$ and $\xi_z^0(k)$ is the Fourier transformation of the initial disturbance $\xi_z^0(y)$. We used the symmetric ($\xi_z^0(y) = \xi_z^0(-y)$) and antisymmetric ($\xi_z^0(y) = -\xi_z^0(-y)$) initial disturbances in form

$$\xi_z^0(y) = \exp(-y^2), \xi_z^0(y) = \sin(y)\exp(-y^2) \tag{17}$$

to model the perturbations for cases with different symmetries. From obtained ξ_z we can determine other parameters of the current sheet (components of the displacement vector, velocity, and magnetic field) using MHD equations:

$$-ik\xi_y + \frac{\partial \xi_z}{\partial z} = 0\,; \qquad \mathbf{v} = \frac{\partial \xi}{\partial t}\,; \qquad \delta\mathbf{B} = \mathrm{curl}[\xi\times\mathbf{B_0}]\,, \tag{18}$$

where $\mathbf{B_0}$ is the background magnetic field.

After analyzing the plasma and magnetic field variations for different initial disturbances and at different observation points, we found out that the initial perturbation (localized somewhere in the center of the current sheet, here at $Z = 0, Y = 0$) generates the localized propagating waves. These waves move from the center to the flanks of the current sheet with geometry depending on the mode: in the kink (sausage) mode the plasma vertical displacements change antisymmetrically (symmetrically) relative to $Z = 0$. Also, the propagation (group) velocity will be different for each mode, its magnitude is approximately twice as large for the kink mode.

In addition to vertical motion of the current sheet, the plasma elements participate in quasi-circular motions in the Z-Y plane during the wave propagation. In other words the plasma elements make smoothly damping oscillations near the equilibrium state, like in the usual wave at the surface of water. We are interested in this motions because the direction of the rotation is opposite for the kink and sausage modes; therefore, it can be used for distinguishing the modes.

According to computations made for the localized source (at $Y = 0, Z = 0$), the plasma rotation pattern is different in four quadrants (behavior is conserved in each quadrant), relative to the neutral sheet and the source location (see Figure 3). The patterns for kink and sausage modes in this figure differ by the opposite

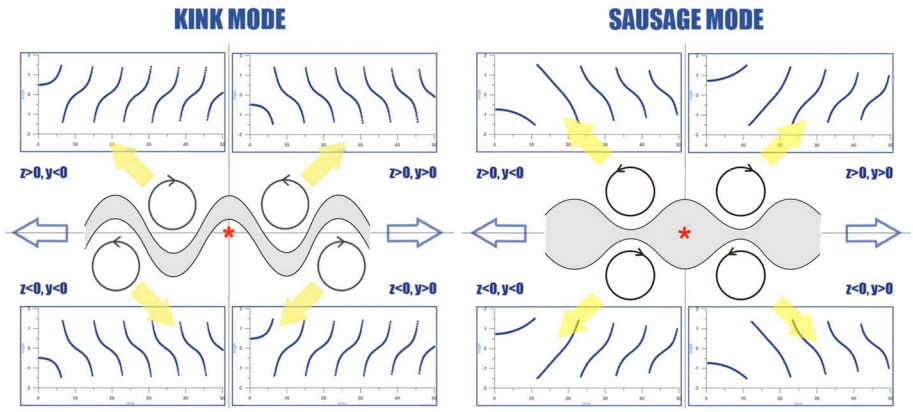

Figure 3. Schematic showing transversal rotation of plasma elements in the flapping wave above and below of the neutral sheet. Left and right parts correspond to the kink and sausage modes, respectively. The middle row shows the schematic representation of the situation. Curved current sheet shape is shown in gray, source location is shown by the red star, and the wave propagation directions are shown by blue arrows. Circles with arrows show how the elements of plasma move in specific quadrant for presented configuration. Top and bottom rows show the periodograms (azimuthal angle in radians versus time) for corresponding four quadrants of *YZ* plane.

direction of rotation. The modeling shows that rotation of the vectors does not depend on the type of initial disturbance, presented by equations (17).

For convenience we can plot the phase angle of the velocity vector V_{yz} or magnetic field vector B_{yz} (vectors in *YZ* plane) as a function of time. Such plot shows the family of the tilted lines, each line corresponds to one period of the V_{yz} rotation, as presented in Figure 3. In this case the tilt sign indicates the direction of the plasma element rotation: the lines will be inclined to the right in case of clockwise rotation and vice versa in case of counterclockwise rotation. So these lines will be inclined in opposite sides for kink and sausage modes in each point. Such data presentation facilitates the detection of periodicity in the experimental data. The line slope characterizes the fundamental parameters of the model, including the double-gradient frequency and corresponding quasiperiod.

3. Observations

Here we show the fortunate event when the configuration of THEMIS probes was optimal for the identification of the flapping mode and investigation of the transversal plasma motions. It occurred on 5 March 2008 in the middle of continuously disturbed time period ($AL \sim 300$–500 nT). Three THEMIS probes *P*1 (at $[-16.2, 2.6, -1.6]R_e$ GSM, taken at 1000 UT), *P*2 (at $[-13.5, 2.2, -2.3]R_e$) and *P*4 (at $[-10.9, 2.2, -2.2]R_e$) stayed near the tail axis in nearly radially aligned configuration. Between 0930 and 1100 UT they observed nearly synchronous large B_x variations (Figure 4, first row) resembling the flapping waves. They cannot be reliably identified as kink waves without more analysis, because B_x was predominantly negative and the THEMIS probes did not cross often the neutral sheet.

Although being so close to *P*4, the probes *P*3 (at $[-10.4, 1.1, -1.9]R_e$) and *P*5 (at $[-9.0, 3.6, -2.3]R_e$) show no synchronous B_x variations (Figure 4, second row). However, as shown by the arrows on this plot, some similarity between time shifted wave forms can be noticed at *P*5, *P*4, and *P*3, suggesting a dawnward propagation of these features in the plasma sheet. In summary, in this fortuitous geometry the THEMIS probes observed a riffle-like perturbation (long in the radial direction and short in cross-tail direction), propagated dawnward, which resembles much the well-known properties of the flapping waves. This configuration allows to investigate further the mode properties.

The choice of proper coordinate system is essential, it can been obtained using Minimal Variance Analysis (MVA) [*Paschmann et al.*, 1986]. The new *X* axis has to lie in the plane of magnetic field lines (this plane is inclined to the *XZ* GSM plane because of flaring etc.). We choose one of the maximum variability direction of the magnetic field (calculated for time interval 1010 : 17–1023 : 26 UT from *P*2 data) as the X_{m1} axis, and set the normal to X_{m1} and Z_{GSM} vector plane as the Y_{m1} axis. We checked that the maximum variability directions at all probes are close to the average direction X_{m1}. At the same time this axis is considerably inclined relative to standard *X* (Sun-Earth) line.

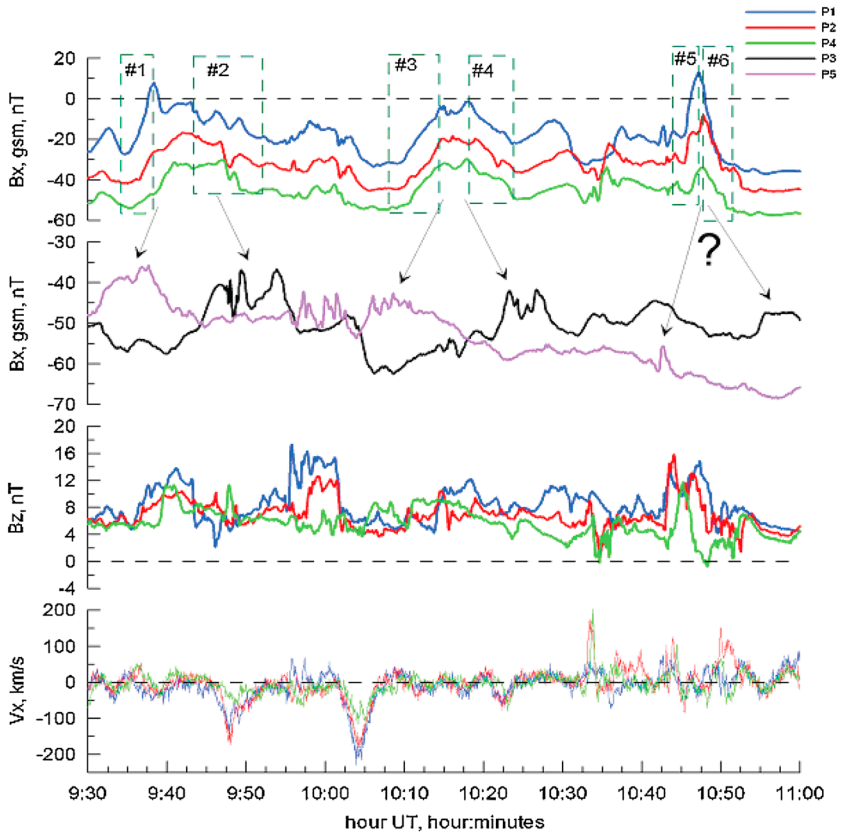

Figure 4. Observations of THEMIS probes on 5 March 2008. (first row) B_x component variations from three radially separated probes P_1, P_2, P_4; (second row) B_x component variations from the azimuthally separated probes P_3 and P_5; (third row) B_z; and (fourth row) ion velocity V_x variations from the probes P_1, P_2, P_4.

Hereafter, we analyzed the time delays dT between the B_x variations using the cross-correlation procedure. For this purpose, we used the oscillations #3/4 which are the most distinct at all probes. Together with spacecraft separation distances dY_{m1} across the magnetic field planes obtained in the new coordinate system, this allows us to estimate the propagation velocity of the flapping wave phase front.

As we can see from the Table 1, the flapping wave velocity is directed toward the dawn flank and is rather small in amplitude (a few tens km/s, as typical for the cross-tail velocities of the flapping waves [e.g., *Runov et al.*, 2005]). One also may notice that the wave velocity decreases when the wave propagates to the morning sector, i.e., opposite to the current (average velocities $P5 \rightarrow P1$, $P5 \rightarrow P2$, and $P5 \rightarrow P4$ are higher comparing to the velocities between $P1 \rightarrow P3$, $P2 \rightarrow P3$, $P3 \rightarrow P4$).

Now we can analyze the behavior of the azimuthal (V_y) and normal (V_z) components of the plasma velocity. Using the average magnetic field coordinate system we can look into the transversal (perpendicular to average **B** direction) magnetic field and plasma flow variations obtained by identical instruments at all THEMIS probes. Here we used the ion plasma moments obtained by combining data from electrostatic analyzer (ESA) and solid state telescope spectrometers [see *Angelopoulos et al.*, 2008]. The velocity values are typically low and noisy, so we use the comparison of observations made by three probes ($P1$, $P2$,

Table 1. Time Delays and Cross-Tail Propagation Velocity Obtained From Cross-Correlation Analysis of the THEMIS Probes P1...P5

	P_5P_1	P_5P_2	P_5P_4	P_5P_3	P_1P_3	P_2P_3	P_4P_3
dY^{m1}, R_e	−2.27	−2.67	−2.01	−2.97	−0.7	−0.3	−0.96
dT, s	426	453	417	945	519	492	528
$V_y^{m1}, km/s$	−34	−38	−30	−20	−28	−4	−12

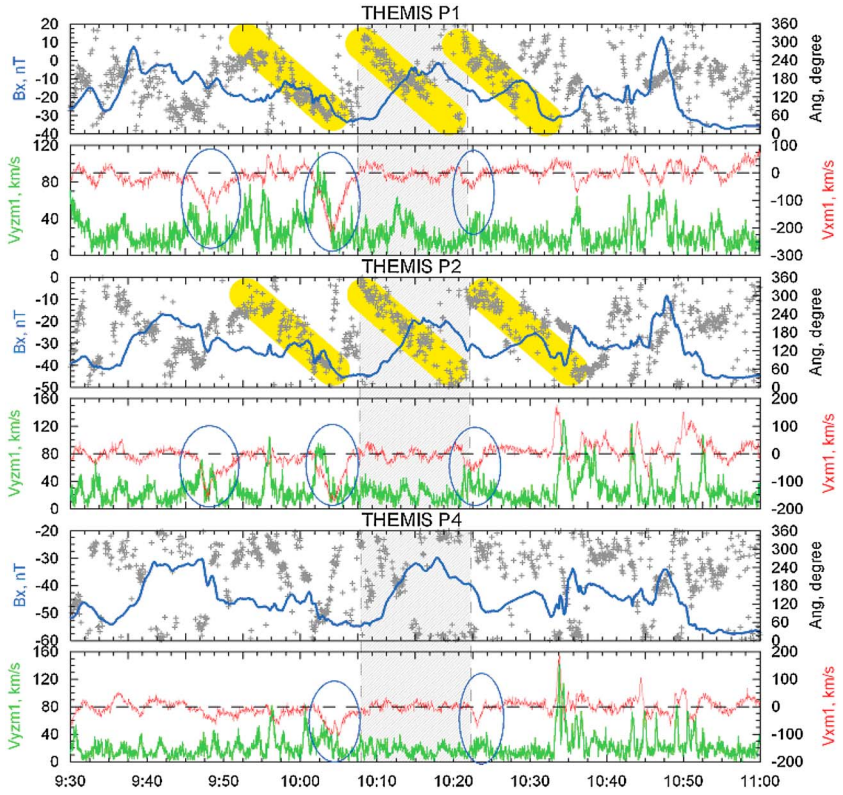

Figure 5. Time variations of the ion velocity azimuthal angle (Ang $=$ $a$tan(V_y/V_z)) compared to the magnetic B_x component, magnitude of transversal velocity (V_{yz}), and V_x component variations for THEMIS probes P_1, P_2, and P_4 on 5 March 2008.

and *P*4 seeing simultaneously the large-scale flapping-like B_x variation) to ensure that we really detect the large-scale flapping-related transversal plasma tube motions. The observed variations can be compared to the theoretical expectations which are schematically presented in Figure 3.

The parameter of primary interest in Figure 5 is the angle (Ang) between the transverse velocity vector and *Z* GSM axis, plotted at 3 s spin resolution. It is plotted in the upper panel for each *P*1, *P*2, and *P*4 probe (only points with $V_{yz} > 15$ km/s were included), with B_x variations is overlapped for comparison. The individual points show clear grouping into the tilted lines (marked by yellow hatching) for the time intervals 0956–1004, 1022–1032, and 1032–1045 UT, manifesting three consecutive periods of steady rotation distinctly observed for *P*1 and *P*2 probes. The V_{yz} magnitudes are shown on the bottom panel (for each of *P*1, *P*2 and *P*4). It can be seen that *P*4 velocities are generally smaller compared to those at *P*1, *P*2 (therefore fewer data points are available), which may partly be responsible for the absence of large-scale rotations seen in *P*4 data. Briefly summarizing, during this event of flapping wave observations, we were able to detect for the first time three consecutive periods of transverse large-scale plasma rotations in the flapping wave. The rotation period for 1004–1022 UT time interval is estimated to be ~12 min as it was described in section 2. The character of rotation corresponds to the theoretical expectations for the kink mode in the case of the tail probe being in the dawn quadrant below the neutral sheet, as consistent with the observations (dawnward propagation and $B_x < 0$).

Similar transverse plasma motions were observed also in the event on 20 December 2007 published by *Runov et al.* [2009]. This event is interesting because the THEMIS probes were located far from midnight (source) unlike in event on 5 March 2008. *Runov et al.* [2009] confirmed the geometry of the flapping waves by using MVA and estimated the average cross-tail velocity of the structure to be − 13– −32 km/s.

Results of the *P*1, *P*2 data analysis similar to that described above but for event on 5 March 2008 are shown in Figure 6. Time axes are shifted by 8 min relative to each other to take into account the propagation effects and facilitate the identification of simultaneous transverse motions (yellow strips). In spite of the noisy pattern, two complete large-scale rotations of plasma elements can be discerned, both are in the clockwise

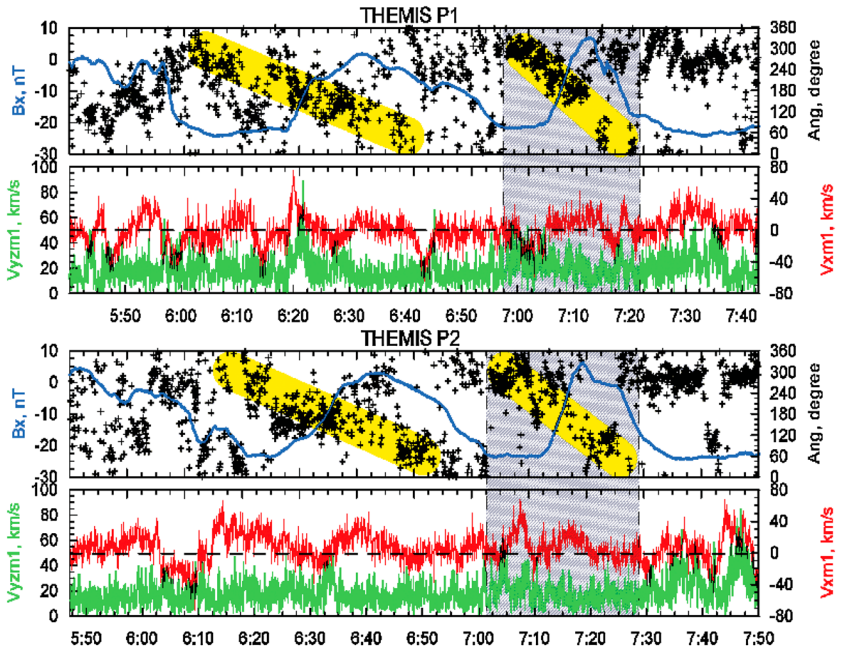

Figure 6. Same as in Figure 4 but for 3 May 2009.

sense, like in the previous case. The marked inclined lines correspond to the quasiperiods of the B_x variations, the long line between 0600 and 0640 UT corresponds to the period of 40 min, the short line between 0657 and 0723 corresponds to $T = 26$ min. These periods are longer than in the previous event. Transverse motions for the P_3, P_4 satellites were not clearly identified. In total, there are some indications of long-period transverse large-scale plasma oscillations, although the data for this event are more noisy compared to the previous event.

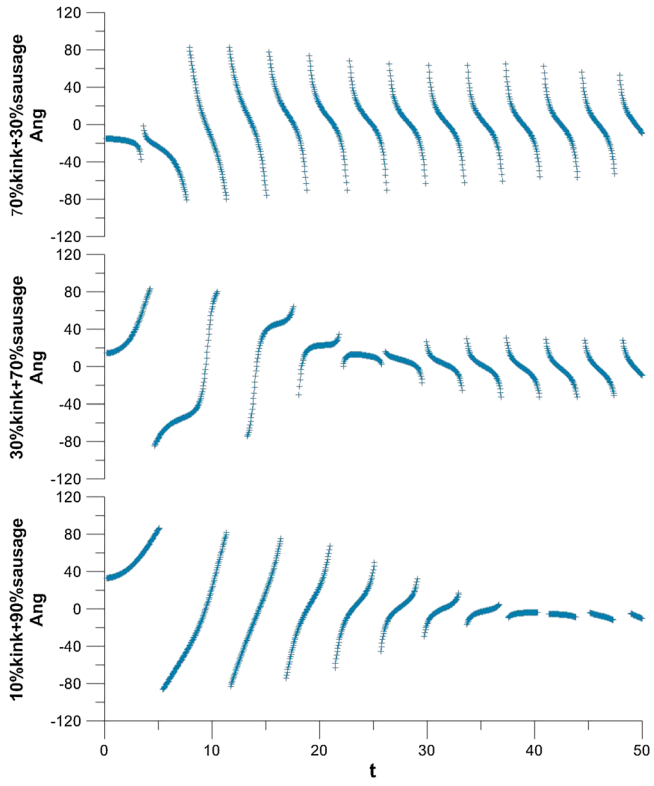

Figure 7. Numerical simulation results for the mixed modes. Periodograms (azimuthal flow angle versus time) are shown in (Y, Z)=(2,0.5) for the different the proportion of the kink mode in the observed wave (10%, 30%, and 70%).

We found the agreement between the model and experimental data, such as similar rotational motion of plasma in the model and the experimental data, with the quasiperiod (in the event on 20 December 2007) being close to the theoretical one (12 and 8.5 min, respectively). Also the tilt of the lines corresponds to the case of the kink mode according to the theoretical prediction. However, it should be noticed that in the model the magnetic field vector shows the similar behavior as the velocity and displacement vectors, particularly the B_{yz} vector hodogram represents the spiral, and the rotation direction changes in different quadrants and for the different modes. By

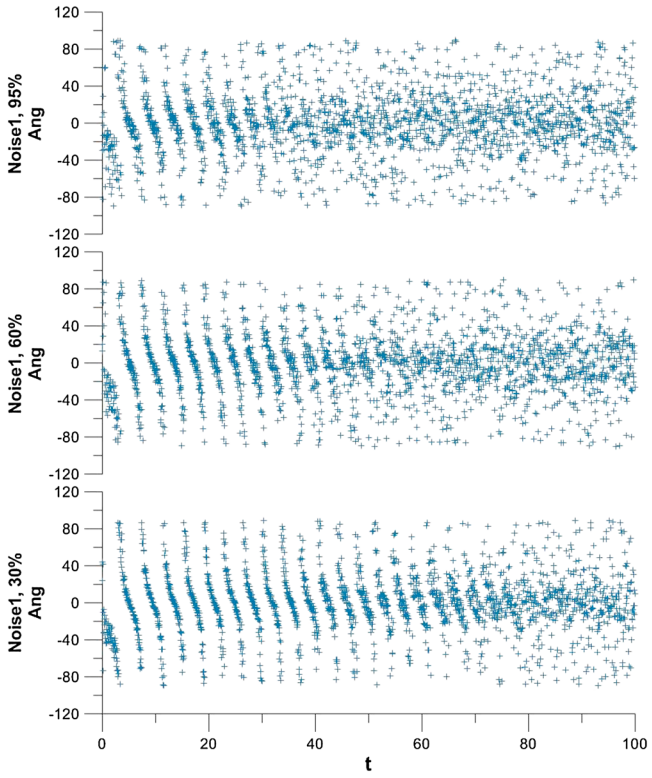

Figure 8. Dependence of the angle of inclination of the velocity vector on time in presence of noise with different amplitudes (30, 60, and 95 % of the signal's amplitude) $z = 0.5z_0, y = 2z_0$.

considering this B_{yz} vector hodogram in the experimental data we were not able to discern clear rotation patterns. At the glance it looks strange, because usually the magnetic field can be obtained with better quality and resolution than velocity data. The answer can be connected with the fact that in the flapping wave the variations of the plasma velocity are proportional to one fluctuating parameter, whereas the magnetic field variations are proportional to the multiple of two fluctuating variables. This implies that for example variations of the velocity Y component ($\rho\frac{\partial v_y}{\partial t} = -\frac{\partial \Pi}{\partial y}$) are proportional to the variations of the total pressure, which is a most stable parameter in the magnetotail. At the same time the magnetic field B_y component variations are $\frac{\partial B_y}{\partial t} = B_z\frac{\partial v_y}{\partial z}$. Though in our linear theory parameter B_z is close to the constant, real B_z is fluctuated and thus B_y proportional to the product of two fluctuated variables. The same can be written for other velocity and magnetic field components. Specifically, the detecting of the periodograms in the velocity data for the flapping oscillations becomes more conveniently than in the magnetic field data.

In the next section we investigate the robustness of the method in case of some interferences, such as mixed modes and presence of the noise or subsources.

4. Mixed Modes

We suppose that oscillations consist of a mixture of linear kink and sausage waves in certain proportion. Time evolution of the parameters (including angles Ang_v and Ang_B) of the mixed mode which are presented in Figure 7 for few different proportions of the modes in the wave.

For 10% of the kink mode and 90% of the sausage mode in the wave the observed parameters behave like in the sausage case for six wave periods, but after some transitional time interval, it turns to kink-like behavior. With 30% of the kink contribution we can see sausage-like behavior only for first three periods, then it behaves like the kink mode. After the percentage of the kink reaches and exceeds 70% we do not see the sausage signatures at all.

Thus, the kink-like behavior can be detected even in presence of small part of the kink mode in the wave, while the sausage mode could be seen clearly only for >50% sausage contribution. The difference is explained by faster propagation (whenever except short initial time interval) of the kink mode as well as by its slower damping rate, so eventually the kink mode dominates over the sausage mode. Such difference may explain why in the most observational studies the flapping oscillations are identified predominantly as the kink mode.

However, we do not have any clear signatures of the mixed modes observation except the changing of the direction of the velocity vector rotation to the opposite. We usually can observe only few periods of the flapping oscillations and thus cannot detect this changing. So if we propose the existence of such mixed oscillations, then the modes determination become ambiguous.

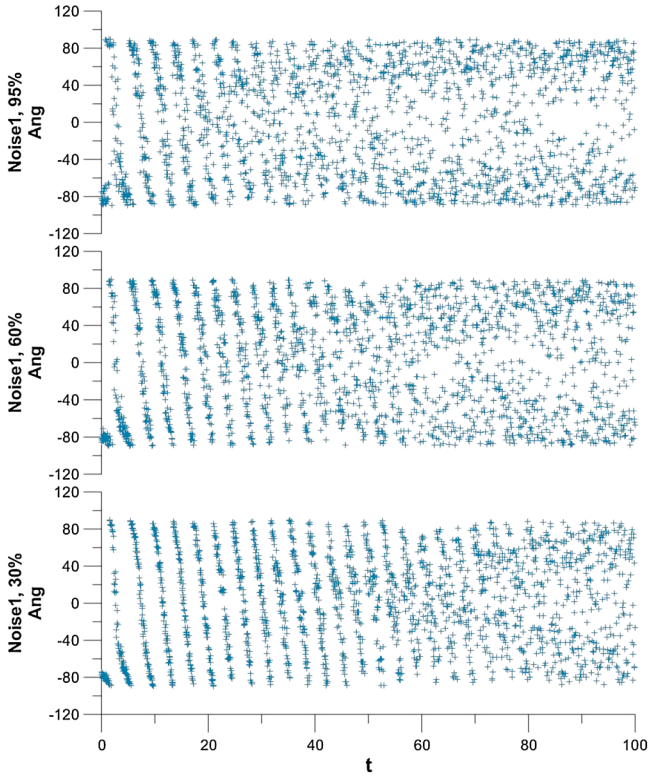

Figure 9. Dependence of the angle of inclination of the magnetic field's vector on time in presence of noise with different amplitudes (30, 60, and 95 % of the signal's amplitude) $z = 0.5z_0, y = 2z_0$.

Thus, the answer to the question: Can we explain the difference in the behavior of magnetic field and velocity vectors in the satellite's data by the existence of the mixed modes? is no. Theoretical time variation of the B_{yz} vector is similar to the V_{yz} variation.

5. Separation of the Modes in Presence of Noise

In this section we check how noise affects on the modes identification mechanism. For the beginning we proposed that we observe the oscillations against the background noise with uniform arrangement and some fixed amplitude. We use the random function to set the noise. The final signal is the linear sum of the pure oscillations with the amplitude $A(t)$ and the noise with the amplitude $A' = m \cdot A_{t=0}$ (we assume that the amplitude of the noise signal is constant for all time interval).

With this noise (permanent for the whole time interval) inclinations corresponded to more belated periods will be broken at less values of coefficient m because of the signal's amplitude decreasing with time. As we can see from Figures 8 and 9 the dependence of vector's **v** and **B** angles of inclination on time breaks at large noise amplitude comparable to the signal's one. On the other hand, developments for speed and magnetic field ruins with one level of the noise.

Another way to take into account the noise is to introduce it into the source term. Noise will be assigned for the displacement at the moment of initiation of the flapping wave. In case of Gaussian initial disturbance (for ξ_z), the signal's amplitude is equal to one half of the current sheet thickness (1 in dimensionless values). So the noise amplitude will be $m_1 \cdot \text{rand}[0, 1]$, where [0, 1] are the limits of the function "rand" and m_1 defines the noise's amplitude. Values of the speed's and magnetic field's noise amplitudes are related in this case and the initial disturbance looks like

$$\xi_0 = Ce^{-a^2y^2} + m_1 \cdot \text{rand}[0, 1] \tag{19}$$

Using the initial disturbance (19) we can get the parameters of the flapping oscillations from the usual procedure which was described in section 3. If we slowly change the noise's amplitude from 0 to maximum we can notice that the dependence for the magnetic field breaks earlier than for the velocity. Destruction occurs in the presence of noise with the order about 15 % of signal's amplitude (Figures 10 and 11).

It is evident that, in reality, both methods of the noise assigning should be used. If we add the noise from the first case to the noise from the second case, then destruction of the dependence will accelerate, but inclinations for magnetic field will still ruin faster.

To find out how the influence of the noise changes in response to location of the point of observation, we propose that noise's level stay about similar in rather wide region in *YZ* plane. In our model the disturbances damp fast in *Z* direction in distances ~2–3 R_e from the current sheet. Apparently, in regions close to the sheet the noise magnitude consist smaller part of the amplitude of the signal than in distant regions. So the Ang(t) dependence could be found in the limited distance from the sheet which could be calculated

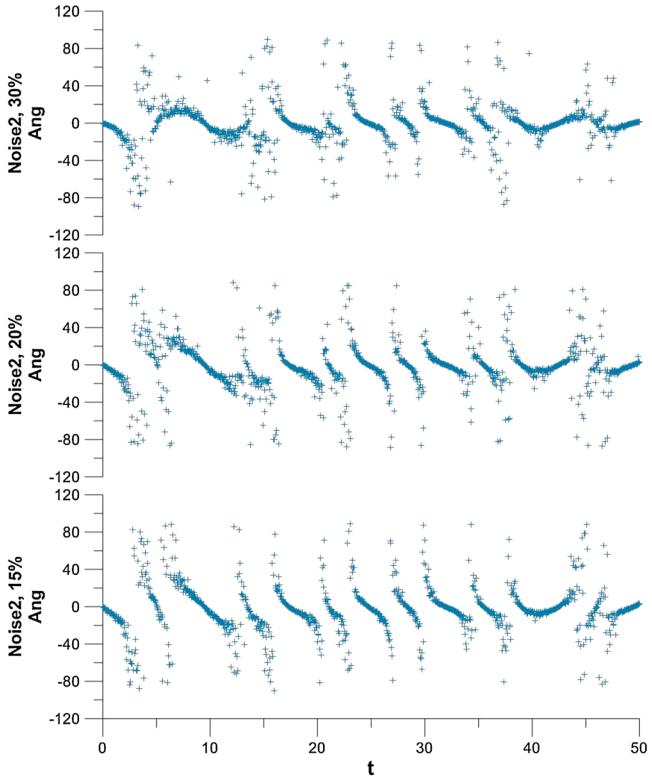

Figure 10. Dependence of the angle of inclination of the velocity's vector on time in presence of noise with different amplitudes (15, 20, and 30 % of the signal's amplitude), second method of the noise's introducing, $z = 0.5z_0, y = 2z_0$.

using signal's amplitude at the center of the current sheet and the noise's amplitude. Along the Y axis (across the magnetic field lines) disturbance expands with slowly changing amplitude, thus inclinations should be observed in the large distance from the source. In numerical model with the noise's amplitude about 20 % of the signal the inclinations are seen at distances as large as about 8 R_e.

6. Implications of Short-Duration Appearance of Inverse Gradient

As we noticed in section 2 there are two possible regimes of the perturbations in the current sheet [*Erkaev et al.*, 2007, 2008]. In the first case (positive double gradient) the wave propagates in the plasma sheet, and our previous discussion concerned this regime which is commonly realized in the real magnetotail. The second case (negative double gradient) corresponds to the instability. In this regime "fingers" grow from the small fluctuations and do not propagate.

Recently *Petrukovich et al.* [2013] analyzed simultaneous observations of radially separated Cluster probes and found that, whereas the positive $\frac{\partial B_z}{\partial x} \cdot \frac{\partial B_x}{\partial z} > 0$ gradient is a norm, short intervals (1–10 min) of inverse negative gradients $\frac{\partial B_z}{\partial x} \cdot \frac{\partial B_x}{\partial z} < 0$ are sometimes observed in the magnetotail. This can have some important consequences.

Based on short-lived nature of inverse gradient events we can propose the following scheme for the generation of the flapping oscillations in the magnetotail. When the inverse gradient appears, always existing small fluctuations grow up due to double-gradient instability. After short time (about few minutes), they grow large enough to produce observable finger-like perturbations. If the magnetic field gradient suddenly changes the sign, these perturbations stop to grow and give rise to the propagating flapping waves.

For illustration we use a simplification. We set the gradients as constant for whole instability and wave intervals. In the first short period of the inverse gradient the initial fluctuations grow up with the instability mechanism. Then we change the gradient to the positive value abruptly and use the wave mechanism at a later stage.

We suppose that initially the biggest disturbances to be localized near the tail center ($Y = 0$) and additional smaller ones to be near the flanks (to mimic the multiple sources or noise). Here we consider just a couple of additional non-overlapping fluctuations (at the $Y = 9$ and at the $Y = -8$) and propose that oscillations belong to the kink mode. In Figure 12 (top) we show the time-evolving shape of the current sheet $\xi_z(y)$ in case of three sources during the instability stage. Equations for the displacement and velocity components in case of instability were obtained by changing of the real frequency $\omega(k)$ to the pure imaginary frequency or increment $\gamma(k)$ in the solution of the flapping equation

$$\xi_z(t, y, z) = \frac{R_e}{2\pi} \int_{-\infty}^{\infty} \xi_z^0(k) \cos(\lambda(k)z) e^{\gamma(k)t - iky} \mathrm{d}k \tag{20}$$

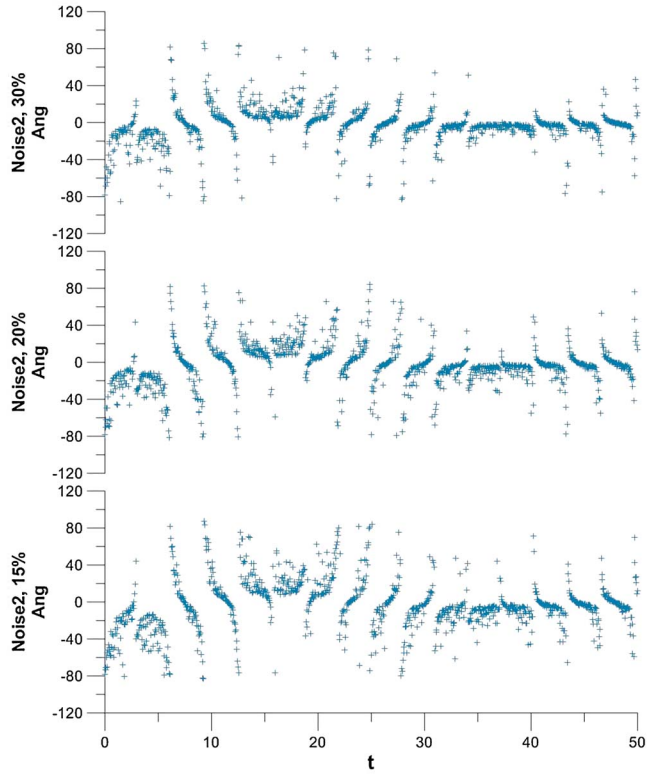

Figure 11. Dependence of the angle of inclination of the magnetic field's vector on time in presence of noise with different amplitudes (15, 20, and 30 % of the signal's amplitude), second method of the noise's introducing, $z = 0.5z_0, y = 2z_0$.

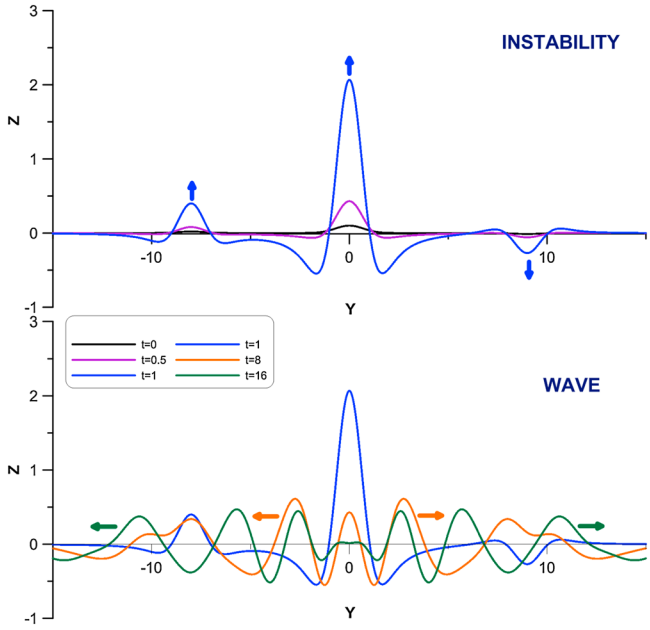

Figure 12. Simulation of the fluctuations evolution: shape of the current sheet in the different times ($\xi_z(y)$). The main source with amplitude A_0 located at $Y = 0$ and subsources located at $Y = 9$ (amplitude $A = -0.75A_0$) and at $Y = -8$ ($A = 0.5A_0$). The point of observation is at $(Y, Z) = (2, 0.5)$. (top) The instability stage (starts in $t = 0$ and continue to $t = 4$, time unit is $T = (\omega_f)^{-1}$) and (bottom) the next wave stage (from $t = 4$ to $t = 64$).

The dependence of this increment $\gamma(k)$ on k is the same as for the dispersion $\omega(k)$, thus we can just change the harmonic oscillations to the exponential growth [*Erkaev et al.*, 2007, 2008].

At $t = 1$ we change the sign of the gradient (turn to the stable case) so these previously increased fluctuations became the initial disturbances of the propagating wave. During the second time interval we calculate parameters of the current sheet by the wave case procedure ($t = 8, 16$ in Figure 12, bottom). Initially, we see some interference between the sources and primary motion from the center of the sheet to the flanks, and after some time interval we see only the wave propagated from the main source.

At the next step we investigate how does the inclusion of a few sources influence the possibility of mode determination by analyzing the behavior of the velocity vector azimuthal angle (periodogram)(Figure 13). While the displacement amplitudes of the additional sources stay small (less than a half) compared to the amplitude of the main source, dependence of the velocity vector on time remains nearly unchanged. If we increase the initial amplitudes then the separation of the modes become troublesome (dependent on the observation point).

For the amplitudes about $0.5A_0$ to $0.8A_0$ and point of observation located between the sources, we can determine just few lines (like in experimental data) and for the bigger amplitude we cannot determine them at all. Mechanism of the modes separation will be crashed in the same way if the distance between sources decreases. This statement is illustrated in Figure 13. If we shift the point of observation out from the region between the sources then Ang(t) dependence will be similar to the one of the one source case.

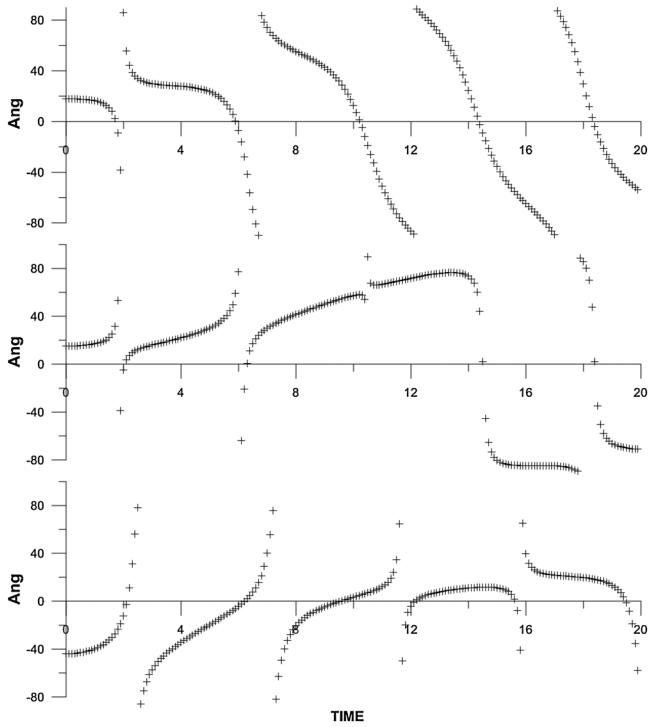

Figure 13. Periodograms for the case of three sources. (top) Corresponds to the case similar to illustrated in Figure 12. The main source with amplitude A_0 is located at $Y = 0$. Subsources amplitudes equal $-0.75A_0$ for the fluctuation at $Y = 7$ and $0.5A_0$ for the fluctuation at $Y = -6$. (middle) Subsources are located at the same places, but amplitudes are bigger, $A = -0.95A_0$ for the fluctuation at $Y = 7$ and $A = 0.95A_0$ for the fluctuation at $Y = -6$. (bottom)We illustrate the case of the distance decreasing. Subsources have the amplitudes equal to the ones from Figure 13 (top), but moved from $Y = -6$ to $Y = -3$ and from $Y = 7$ to $Y = 5$. The point of observation is located at $(Y, Z) = (4.0, 0.5)$.

To conclude the instability play the ambiguous role in the current sheet dynamics. On the one hand, existence of the inverse gradient produces a lot of problems for the detection and analysis of the flapping waves and makes the modes separation mechanism hard to apply. This was shown in the present paper for the simplified model with few initial disturbances and the picture supposed to be even more complex for the real current sheet. Thus, we can conclude that probably the main difficulty in mode's separation is not the noise but the existence of the multiple sources of the oscillations. From the other hand, this inverse gradient mechanism as well as reconnection proposed by *Sergeev et al.* [2003] can be the powerful source of the flapping wave appearance.

7. Conclusions

In this paper we investigated the possibility of the flapping modes separation based on the analysis of the azimuthal (V_y) and normal (V_z) components of plasma velocity. The velocity vector rotates clockwise or counterclockwise and direction of this rotation is different for the kink and sausage modes at the all points of space. We used the dependence of the angle of inclination ($a\tan(V_y/V_z)$) on time, which represents the series of the lines inclined differently for the different modes. From the angle of inclination of these lines we obtain the double-gradient frequency. The relevant model was based on double gradient of magnetic field.

We shown the fortunate event (it occurred on 5 March 2008) in which the configuration of THEMIS probes constellation was optimal for the identification and investigation of the flapping-like waves. During this event of flapping wave observations, we were able to detect for the first time three consecutive periods of transverse large-scale plasma rotations in the flapping wave. The rotation period for 1004–1022 UT time interval was estimated to be ~12 min. The character of rotation corresponded to the theoretical expectations for the kink mode in the case of the tail probe being in the dawn quadrant below the neutral sheet, as consistent with the observations (dawnward propagation and $B_x < 0$).

It was found out that the tilt of the lines corresponds to the case of the kink mode according to the theoretical model as it was expected. However, it should be noticed that in the model, the magnetic field vector shows the similar behavior as the velocity and displacement vectors, but the tilted lines in the angle between **B** and Z_{GSM} dependence on time was not found out in the experimental data. For this purpose we investigated the robustness of the method in case of the mixed modes, in the presence of noise and also we analyzed the case of instability.

We found out that the modes separation mechanism can be crashed by the presence of the enough strong noise. Moreover, the behavior of the velocity vector is more stable than the behavior of the magnetic field vector. Even more than noise, the existence of the multiple sources of the oscillations could be the main

difficulty in mode's separation. This multiple sources supposed to appear in many events because of inverse gradients (instability) existence.

Acknowledgments

We thank C. W. Carlson and J. P. McFadden for use of THEMIS ESA data; K. H. Glassmeier, U. Auster, and W. Baumjohann for the use of FGM data provided under the lead of the Technical University of Braunschweig and with financial support through the German Ministry for Economy and Technology and the German Center for Aviation and Space (DLR) under contract 50 OC 0302. The work was partly supported by SPbU grant 11.38.84.12, by RFBR grants 12-05-00152-a and 12-05-00918-a, and by the grant for support of leading Scientific schools 2836.2014.5. The work of S. Dubyagin and N. Ganushkina was partly supported by the Academy of Finland. This work was supported by the Austrian Science Fund (FWF): I193-N16. N.V.E acknowledges the support by the International Space Science Institute (ISSI, Switzerland) and discussions within the ISSI Team 214 on Flow-Driven Instabilities of the Sun-Earth System. The research has received funding also from the European Union Seventh Framework Programme [FP7/2007-2013] under grant agreement 269198-Geoplasmas (Marie Curie International Research Staff Exchange Scheme) and 218816 (SOTERIA project).

Masaki Fujimoto thanks the reviewers for their assistance in evaluating this paper.

References

Angelopoulos, V., et al. (2008), First Results from the THEMIS Mission, *Space Sci. Rev.*, *141*, 453–476, doi:10.1007/s11214-008-9378-4.

Artemyev, A., and I. Zimovets (2012), Stability of current sheets in the solar corona, *Sol. Phys.*, *277*, 283–298, doi:10.1007/s11207-011-9908-1.

Daughton, W. (1998), Kinetic theory of the drift kink instability in a current sheet, *J. Geophys. Res.*, *103*(A12), 29,429–29,443, doi:10.1029/1998JA900028.

Daughton, W. (1999), Two-fluid theory of the drift kink instability, *J. Geophys. Res.*, *104*(A12), 28,701–28,707, doi:10.1029/1999JA900388.

Erkaev, N. V., V. S. Semenov, and H. K. Biernat (2007), Magnetic double-gradient instability and flapping waves in a current sheet, *Phys. Rev. Lett.*, *99*, 235,003, doi:10.1103/PhysRevLett.99.235003.

Erkaev, N. V., V. S. Semenov, and H. K. Biernat (2008), Magnetic double gradient mechanism for flapping oscillations of a current sheet, *Geophys. Res. Lett.*, *35*, L02111, doi:10.1029/2007GL032277.

Erkaev, N. V., V. S. Semenov, I. V. Kubyshkin, M. V. Kubyshkina, and H. K. Biernat (2009a), MHD model of the flapping motions in the magnetotail current sheet, *J. Geophys. Res.*, *114*, A03206, doi:10.1029/2008JA013728.

Erkaev, N. V., V. S. Semenov, I. V. Kubyshkin, M. V. Kubyshkina, and H. K. Biernat (2009b), MHD aspect of current sheet oscillations related to magnetic field gradients, *Ann. Geophys.*, *27*(1), 417–425, doi:10.5194/angeo-27-417-2009.

Erkaev, N. V., V. S. Semenov, and H. K. Biernat (2010), *Phys. Plasmas*, *17*, 060,703, doi:10.1063/1.3439687.

Forsyth, C., M. Lester, R. C. Fear, E. Lucek, I. Dandouras, A. N. Fazakerley, H. Singer, and T. K. Yeoman (2009), Solar wind and substorm excitation of the wavy current sheet, *Ann. Geophys.*, *27*, 2457–2474, doi:10.5194/angeo-27-2457-2009.

Golovchanskaya, I. V., and Y. P. Maltsev (2005), On the identification of plasma sheet flapping waves observed by Cluster, *Geophys. Res. Lett.*, *32*, L02102, doi:10.1029/2004GL021552.

Karimabadi, H., P. L. Pritchett, W. Daughton, and D. Krauss-Varban (2003), Ion-ion kink instability in the magnetotail: 2. Three-dimensional full particle and hybrid simulations and comparison with observations, *J. Geophys. Res.*, *108*(A11), 1401, doi:10.1029/2003JA010109.

Korovinskiy, D. B., A. Divin, N. V. Erkaev, V. V. Ivanova, I. B. Ivanov, V. S. Semenov, G. Lapenta, S. Markidis, H. K. Biernat, and M. Zellinger (2013), MHD modeling of the double-gradient (kink) magnetic instability, *J. Geophys. Res. Space Physics*, *118*(3), 1146–1158, doi:10.1002/jgra.50206.

Mazur, N. G., E. N. Fedorov, and V. A. Pilipenko (2012), Dispersion relation for ballooning modes and condition of their stability in the near-earth plasma, *Geomag. Aeron.*, *52*(5), 603–612.

Ness, N. F. (1965), The Earth's magnetic tail, *J. Geophys. Res.*, *70*, 2989–3005, doi:10.1029/JZ070i013p02989.

Panov, E. V., V. A. Sergeev, P. L. Pritchett, F. V. Coroniti, R. Nakamura, W. Baumjohann, V. Angelopoulos, H. U. Auster, and J. P. McFadden (2012), Observations of kinetic ballooning/interchange instability signatures in the magnetotail, *Geophys. Res. Lett.*, *39*, L08110, doi:10.1029/2012GL051668.

Paschmann, G., I. Papamastorakis, W. Baumjohann, N. Sckopke, C. W. Carlson, B. U. Sonnerup, and H. Lühr (1986), The magnetopause for large magnetic shear: AMPTE/IRM observations, *J. Geophys. Res.*, *91*, 11,099–11,115, doi:10.1029/JA091iA10p11099.

Petrukovich, A. A., T. I. Zhang, W. Baumjohann, R. Nakamura, A. Runov, A. Balogh, and C. Carr (2006), Oscillatory magnetic flux tube slippage in the plasma sheet, *Ann. Geophys.*, *24*, 1695–1704.

Petrukovich, A. A., A. V. Artemyev, R. Nakamura, V. Panov, and W. Baumjohann (2013), Cluster observations of $\partial B_z/\partial x$ during growth phase magnetotail stretching intervals, *J. Geophys. Res. Space Physics*, *118*, 5720–5730, doi:10.1002/jgra.50550.

Ricci, P., G. Lapenta, and J. U. Brackbill (2004), Structure of the magnetotail current: Kinetic simulation and comparison with satellite observations, *Geophys. Res. Lett.*, *31*, L06801, doi:10.1029/2003GL019207.

Runov, A., et al. (2005), Electric current and magnetic field geometry in flapping magnetotail current sheets, *Ann. Geophys.*, *23*, 1391–1403.

Runov, A., et al. (2006), Local structure of the magnetotail current sheet: 2001 Cluster observations, *Ann. Geophys.*, *24*, 247—262.

Runov, A., V. Angelopoulos, V. A. Sergeev, K.-H. Glassmeier, U. Auster, J. McFadden, D. Larson, and I. Mann (2009), Global properties of magnetotail current sheet flapping: THEMIS perspectives, *Ann. Geophys.*, *27*, 319–328s.

Sergeev, V., et al. (2003), Current sheet flapping motion and structure observed by Cluster, *Geophys. Res. Lett.*, *30*(6), 1327, doi:10.1029/2002GL016500.

Sergeev, V., A. Runov, W. Baumjohann, R. Nakamura, T. L. Zhang, A. Balogh, P. Louarn, J.-A. Sauvaud, and H. Reme (2004), Orientation and propagation of current sheet oscillations, *Geophys. Res. Lett.*, *30*, L05807, doi:10.1029/2003GL019346.

Sergeev, V. A., A. Rounov, W. Baumjohann, R. Nakamura, T. L. Zhang, S. Apatenkov, A. Balogh, H. Rème, and J.-A. Sauvaud (2006a), Cluster results on the magnetotail current sheet structure and dynamics, in *Proceedings, Cluster and Double Star Symposium—5th Anniversary of Cluster in Space*, edited by K. Fletcher, pp. P9.2, ESA SP 598, Noordwijk.

Sergeev, V. A., D. A. Sormakov, S. V. Apatenkov, W. Baumjohann, R. Nakamura, A. V. Runov, T. Mukai, and T. Nagai (2006b), Survey of large-amplitude flapping motions in the midtail current sheet, *Ann. Geophys.*, *24*, 2015–2024.

Shen, C., et al. (2003), Analyses on the geometrical structure of magnetic field in the current sheet based on Cluster measurements, *J. Geophys. Res.*, *108*(A5), 1168, doi:10.1029/2002JA009612.

Sitnov, M. I., M. Swisdak, J. F. Drake, P. N. Guzdar, and B. N. Rogers (2004), A model of the bifurcated current sheet: 2. Flapping motion, *Geophys. Res. Lett.*, *31*, L09805, doi:10.1029/2004GL019473.

Volwerk, M., et al. (2013), Comparative magnetotail flapping: An overview of selected events at Earth, Jupiter and Saturn, *Ann. Geophys.*, *31*, 817–833, doi:10.5194/angeo-31-817-2013.

Zelenyi, L. M., A. V. Artemyev, A. A. Petrukovich, R. Nakamura, and H. V. Malova (2009), Low frequency eigenmodes of thin anisotropic current sheets and Cluster observations, *Ann. Geophys.*, *27*, 861–868.

Zhang, T. L., W. Baumjohann, R. Nakamura, A. Balogh, and K.-H. KGlassmeier (2002), A wavy twisted neutral sheet observed by CLUSTER, *Geophys. Res. Lett.*, *29*(19), 1899, doi:10.1029/2002GL015544.